Developmental Cognitive Neuroscience 34 (2018) 27–33

Contents lists available at ScienceDirect

Developmental Cognitive Neuroscience

journal homepage: www.elsevier.com/locate/dcn

Mechanical properties of the *in vivo* adolescent human brain

Grace McIlvain[a], Hillary Schwarb[b], Neal J. Cohen[b], Eva H. Telzer[c], Curtis L. Johnson[a,*]

[a] Department of Biomedical Engineering, University of Delaware, Newark, DE, United States
[b] Beckman Institute for Advanced Science and Technology, University of Illinois, Urbana, IL, United States
[c] Department of Psychology and Neuroscience, University of North Carolina, Chapel Hill, NC, United States

ARTICLE INFO

Keywords:
Magnetic resonance elastography
Brain
Stiffness
Viscoelasticity
Adolescent
Pediatric

ABSTRACT

Viscoelastic mechanical properties of the *in vivo* human brain, measured noninvasively with magnetic resonance elastography (MRE), have recently been shown to be affected by aging and neurological disease, as well as relate to performance on cognitive tasks in adults. The demonstrated sensitivity of brain mechanical properties to neural tissue integrity make them an attractive target for examining the developing brain; however, to date, MRE studies on children are lacking. In this work, we characterized global and regional brain stiffness and damping ratio in a sample of 40 adolescents aged 12–14 years, including the lobes of the cerebrum and subcortical gray matter structures. We also compared the properties of the adolescent brain to the healthy adult brain. Temporal and parietal cerebral lobes were softer in adolescents compared to adults. We found that of subcortical gray matter structures, the caudate and the putamen were significantly stiffer in adolescents, and that the hippocampus and amygdala were significantly less stiff than all other subcortical structures. This study provides the first detailed characterization of adolescent brain viscoelasticity and provides baseline data to be used in studying development and pathophysiology.

1. Introduction

The study of viscoelastic mechanical properties of the healthy adult brain, through magnetic resonance elastography (MRE) (Muthupillai et al., 1995), has led to a quantitative understanding of the *in vivo* stiffness of neural tissue (Hiscox et al., 2016). Through advances in MRE technology, reports of reliable regional mechanical properties in the adult brain have been published, including data on different cerebral lobes (Murphy et al., 2013) and subcortical gray matter structures (Johnson et al., 2016). Stiffness and damping ratio data collected through MRE has theoretically and experimentally been correlated with microstructural brain health (Hiscox et al., 2016) as it provides a sensitive quantitative measure of biological factors such as white matter myelination and number of neurons (Sack et al., 2013). MRE studies of the adult brain have found brain stiffness to be affected by different neurodegenerative diseases (Murphy et al., 2016; Romano et al., 2012; Streitberger et al., 2012), and have also revealed correlations with fitness measures and cognitive tasks (Johnson et al., 2018; Schwarb et al., 2017, 2016). Adult brain MRE studies have also revealed changes in mechanical properties with age (Arani et al., 2015; Hiscox et al., 2018; Sack et al., 2011). Specifically, several studies have revealed a softening of brain tissue as it ages, with annual changes in stiffness between −0.3 and −1.0%, demonstrating how mechanical properties can be used to probe structural changes in the healthy brain.

Although considerable MRE data exists for the adult brain, no MRE studies examining the developing brain have yet been reported, despite the potential for mechanical properties to increase our knowledge of how brain structure matures (Johnson and Telzer, 2017). The brain undergoes many cellular level structural changes during adolescence, including volume variations both in total size and structure proportion, as well as a redistribution of gray and white matter (Gogtay et al., 2004; Raznahan et al., 2014) and myelination of white matter tracts (Lebel et al., 2017). Given significant structural brain changes during development, and the sensitivity of mechanical properties to neural tissue microstructure, MRE may provide a unique contrast for imaging the developing brain. It has been seen that MRE provides a complementary contrast compared to volumetric analysis for examining complex interactions of neuronal components (Wuerfel et al., 2010). Previous brain MRE studies have demonstrated the potential for measuring mechanical properties of the developing brain as these measures are expected to have higher sensitivity than many other common imaging contrasts (Mariappan et al., 2010).

The viscoelastic brain properties commonly reported by MRE are related to both the microstructural composition and organization of neural tissue (Sack et al., 2013). This is reflected in animal studies with MRE that have found changes in mechanical properties correlating with

* Corresponding author at: 150 Academy St, Newark, DE 19716, United States.
E-mail address: clj@udel.edu (C.L. Johnson).

https://doi.org/10.1016/j.dcn.2018.06.001
Received 13 May 2018; Accepted 5 June 2018
Available online 10 June 2018

microstructural tissue characteristics, such as number of neurons in models of neurogenesis (Hain et al., 2016; Klein et al., 2014) and ischemic stroke (Freimann et al., 2013). Notably, viscoelastic properties measured with MRE are also sensitive to demyelination and remyelination (Schregel et al., 2012). Myelin specific MRI sequences have been developed to image the water content in the lipid bilayers of myelinated axons; however, these methods may artificially overestimate myelination (Alonso-Ortiz et al., 2015; Wang, 2012; West et al., 2016), and thus alternative and complementary approaches to examining myelin content are needed. Myelination of axons increases their mechanical strength (Shreiber et al., 2009), and brain stiffness increases with the number of intact myelinated axons (Weickenmeier et al., 2017), thus giving rise to white matter being stiffer than gray matter (Budday et al., 2015). The volume and proportion of white matter increases through development into adulthood (Paus et al., 2001), and local myelin distribution changes with age and functional need (Lenroot and Giedd, 2006), thus mechanical properties are expected to reflect these changes.

The volume and structure of gray matter also changes with development, including synaptogenesis and dendritic pruning, which are related to the maturation of cognitive functions. Gray matter density is often impacted in developmental disorders and their associated cognitive impairments (Toga et al., 2006). Recently, our group has demonstrated that MRE measures of gray matter regions can be highly sensitive to cognitive function, specifically viscoelasticity of the hippocampus as it relates to performance on memory tasks (Schwarb et al., 2017, 2016). This highlights the potential of MRE in mapping brain structure and function through mechanical properties.

This study aims to quantify the viscoelastic mechanical properties of the adolescent human brain *in vivo* using MRE. We report both global and regional property values quantified in lobes of the cerebrum and in subcortical gray matter structures. We further compare these adolescent properties to adult brain property values, collected and processed through a common protocol. To our knowledge, this is the first detailed characterization of the viscoelastic mechanical properties of the adolescent human brain measured *in vivo* with MRE. An understanding of healthy adolescent brain viscoelasticity at age of puberty will increase the knowledge of brain mechanics at an age where little is known about these properties, and can provide baseline data to be used in studying the pathophysiology and longitudinal development of the adolescent brain.

2. Methods

2.1. Participants

A total of 46 (22 male / 24 female) healthy, cognitively normal, right-handed adolescents, 12–14 years old and 20 healthy male, cognitively normal adults, 18–33 years old were included in the study. The adolescent data was collected as a subset of participants from a larger study where only a small portion completed the MRE scan. The adult data used for comparison was of the same subjects for two other adult MRE studies (Johnson et al., 2016; Schwarb et al., 2016) and was reprocessed for the purpose of direct comparison in this paper. Of the 66 collected datasets, four had low signal-to-noise ratio (SNR) (McGarry et al., 2011) or artifacts in the reconstructed property maps and two were determined to be outliers (see *Statistical Analysis* section, below), so the final sample included data from 40 adolescents (19 male / 21 female) and 20 adult males. This study was approved by the University of Illinois at Urbana-Champaign Institutional Review Board and all participants, and guardians of the adolescent participants, gave informed written consent prior to being studied.

2.2. Imaging data acquisition and processing

Each adolescent participant completed an imaging session on a Siemens 3 T Trio MRI scanner (Siemens Medical Solutions; Erlangen, Germany), with a protocol that included a high-resolution, T_1-weighted MPRAGE sequence (magnetization-prepared rapidly-acquired gradient echo; $0.9 \times 0.9 \times 0.9$ mm^3; TR/TI/TE = 1900/900/2.32 ms) for anatomical localization and an MRE acquisition. The MRE experiment involves vibrating the head to generate shear waves with micron-level amplitude that propagate through the brain. These waves are imaged with a phase-contrast motion-encoding MRI sequence synchronized to vibrations. By repeating the acquisition with different synchronization and motion-encoding gradient axes, 3D, full vector, complex displacement fields are captured across the entire brain. These displacement fields are used to estimate the brain mechanical properties through an "inversion" algorithm that uses a model of viscoelastic tissue behavior to create whole-brain property maps (Hiscox et al., 2016; Johnson and Telzer, 2017).

We acquired MRE data using a 3D multislab, multishot spiral sequence (Johnson et al., 2014). The resulting MRE images had $2.0 \times 2.0 \times 2.0$ mm^3 isotropic spatial resolution, and encoded displacements from 50 Hz vibrations delivered to the head *via* pneumatic actuator system with passive pillow driver (Resoundant, Inc.; Rochester, MN). Additional imaging parameters included: field-of-view = 240×240 mm^2; matrix = 120×120; 60 total slices (10 slabs; 8 slices per slab; 25% slab overlap); 1 in-plane spiral shot ($R = 3$); TR/TE = 1800/73 ms; bilateral, flow-compensated, matched-period motion-encoding gradients, 26 m T/m; 4 evenly-spaced phase offsets. Total acquisition time was 6 min. Iterative image reconstruction included field inhomogeneity correction, SENSE parallel imaging, and correction for small motion-induced phase errors between shots for a single imaging volume that may arise from subject motion or variations in applied vibration, as described in (Johnson et al., 2014). Data quality was confirmed after image reconstruction by the octahedral shear strain-based (SNR) (McGarry et al., 2011), where an SNR > 3 is sufficient for stable inversion and reliable property maps. This data quality check excluded datasets with too low displacement amplitude (*i.e.* from lack of sufficient head vibration) or data corrupted from excessive head motion.

The adult participants included in this paper underwent a nearly identical data collection procedure, however with a higher MRE spatial resolution (1.6 mm isotropic voxels). For comparison in this study, the higher resolution data was downsampled to 2.0 mm isotropic voxel size for comparison with the adolescent population. This downsampling occurred prior to inversion (next section) and all data was completely reprocessed using the identical pipeline. We have previously demonstrated that this downsampling had minimal effect on the population values recovered with MRE (Johnson et al., 2016).

The nonlinear inversion algorithm (NLI) was used to estimate brain tissue viscoelastic properties from MRE displacement data (McGarry et al., 2012; Van Houten et al., 2001). NLI returns whole-brain maps of the complex viscoelastic shear modulus ($G = G' + G''$), from which we calculate shear stiffness, $\mu = 2|G|^2/(G' + |G|)$ (Manduca et al., 2001), and damping ratio, $\xi = G''/2G'$ (McGarry and Van Houten, 2008). We also incorporated *a priori* spatial information during inversion through soft prior regularization (SPR) (McGarry et al., 2013) to improve the measures of subcortical gray matter regions. This involves providing masks of each subcortical region (see next section) over which property variation is penalized through SPR during NLI optimization. This is the same pipeline which was previously used for subcortical gray matter property estimation in adults (Johnson et al., 2016; Schwarb et al., 2016), and has been demonstrated to reduce variability in measures potentially arising from contamination of nearby cerebrospinal fluid (CSF).

2.3. Regional data analysis

Masks for mechanical property characterization of neuroanatomical structures were created using standard neuroimaging tools. Lobar

masks for each subject were generated from the standard-space WFU PickAtlas (Maldjian et al., 2003) based on bilateral atlas masks of the cerebrum; cerebellum; frontal, occipital, parietal, and temporal lobes; and deep gray matter and white matter (deep GM/WM). The deep GM/WM comprises the limbic lobe and sublobe regions from the atlas. These atlas regions were first registered to the subject-specific MPRAGE scans using FNIRT (Andersson et al., 2008), then to the MRE data through FLIRT (Jenkinson et al., 2002), both of which are FSL utilities (Jenkinson et al., 2012). Masks of GM, WM, and CSF were also created from the MPRAGE scan using FAST (Zhang et al., 2001) in FSL. After registration of tissue type masks to MRE data, we mitigated direct effects of CSF on lobar stiffness values by removing voxels containing any CSF and analyzed only voxels containing 100% white and gray matter. Subcortical gray matter structures (amygdala, hippocampus, caudate, putamen, pallidum, and thalamus) were automatically segmented from the MPRAGE scan for each subject using FIRST (Patenaude et al., 2011) in FSL. These regional masks were similarly registered to MRE data through FLIRT and were used in NLI through SPR (see above) and to calculate regional properties. SPR was not used on lobes as McGarry et al. (2013) reported that regional homogeneity provided by SPR is only preferable for structures on the subzone scale, and SPR can introduce instability if used on large regions.

2.4. Statistical analysis

All analysis was performed using JMP Pro 13.1.0 (SAS Institute, Inc. Cary, NC). Initially, outliers were eliminated using multivariate robust outlier analysis (10% tail quantile; data excluded at three times the interquartile range); any subject with a stiffness outlier in one or more regions of the brain was eliminated from analysis completely. Through this analysis, we excluded 2 of 42 adolescent datasets, for a total sample of 40 adolescent participants. Repeated measure analysis of variance (ANOVA) tests were performed to test for differences between brain regions, as well as potential dependence of properties on age and sex. Tukey *post hoc* tests compared each brain region pair with significance determined at $p < 0.05$ after correction for multiple comparisons. ANOVAs were performed to test for differences in properties between adult and adolescent populations, followed by individual *post hoc* tests comparing adolescents and adults for each structure with significance determined at $p < 0.05$.

3. Results

Stiffness, μ, and damping ratio, ξ, were calculated for the cerebrum, cerebral lobes, and subcortical gray matter structures in our adolescent population (Fig. 1), and are presented in Tables 1 and 2. Repeated measures ANOVAs, performed separately for both lobes and subcortical structures, and for μ and ξ, indicated significant differences between structures ($p < 0.001$ for all four omnibus tests). *Post hoc* comparisons are described in the following sections. We also included sex in the ANOVA models and found that females had higher stiffness ($p = 0.036$) and lower damping ratio ($p = 0.028$) in subcortical structures; however, there was no significant sex effect in any of the lobes or the subcortical structures after *post hoc* tests. Data for each region by sex in the adolescent population are included as Supplemental information (Tables S1 and S2). We also initially considered age though there were no significant omnibus effects.

3.1. Shear stiffness

Fig. 2 presents μ values for both cerebral lobes and subcortical gray matter structures, which are also shown in Table 1. In general, the cerebrum and cerebral lobes exhibited significantly higher stiffness than the cerebellum. The cerebellum being softer than the cerebrum (2.48 v. 3.13; −20.8%) in adolescents is consistent with previous observations in adults (Johnson et al., 2014; Murphy et al., 2013; Zhang et al., 2011) and in our adult group (2.74 v. 3.23; −15.2%). In adolescents, the lobes did not differ significantly from each other, but the occipital and parietal lobes were both significantly softer than the overall cerebrum. Additionally, deep GM/WM has higher stiffness than all other regions, including the cerebrum (3.49 v. 3.13; 11.5%) in adolescents, which is consistent with previous findings in adults (Murphy et al., 2013) and in our adult group (3.45 v. 3.23; 6.8%).

The deep GM/WM region, as previously discussed, partially encompasses subcortical gray matter structures, which we also analyzed individually. All adolescent subcortical structures except the hippocampus are significantly stiffer than the cerebrum, ranging in values from 3.49 kPa in the amygdala to 4.11 kPa in the caudate

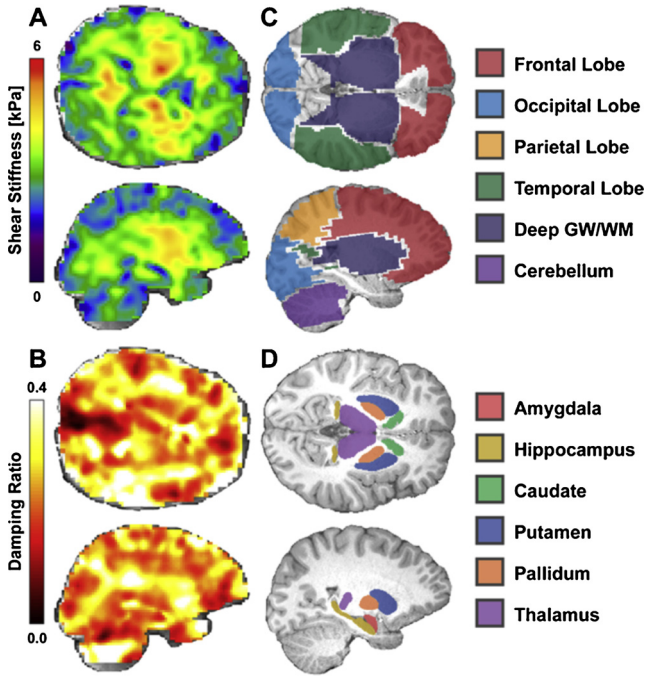

Fig. 1. A) Example shear stiffness map and B) example damping ratio map. C) Lobar ROIs, including frontal (red), occipital (blue), parietal (orange), and temporal (green), along with deep GM/WM (dark blue) and cerebellum (purple). D) Subcortical gray matter ROIs, including amygdala (red), hippocampus (gold), caudate (green), putamen (blue), pallidum (orange), and thalamus (purple) Note: Cerebrum ROI not pictured but encompasses the four cerebral lobes pictured (frontal, occipital, parietal and temporal) and deep GM/WM (For interpretation of the references to colour in this figure legend, the reader is referred to the web version of this article).

Table 1
Shear stiffness, μ, of cerebral lobes and subcortical gray matter structures in adolescents and adults, and Cohen's *d* effect size indicating the difference between populations. Values presented as population mean (standard deviation) in kPa. Significant differences are marked with *.

Region	Adolescent μ	Adult μ	Cohen's *d*
Cerebrum	3.13 (0.31)	3.23 (0.21)	−0.38
Cerebellum	2.48 (0.27)	2.74 (0.21)	−1.06*
Frontal Lobe	2.97 (0.32)	3.11 (0.26)	−0.48
Occipital Lobe	2.80 (0.25)	2.76 (0.26)	0.05
Parietal Lobe	2.84 (0.37)	3.12 (0.52)	−0.68*
Temporal Lobe	3.01 (0.25)	3.16 (0.30)	−0.56*
Deep GM/WM	3.49 (0.44)	3.45 (0.25)	0.09
Amygdala	3.49 (0.41)	3.59 (0.32)	−0.26
Hippocampus	3.25 (0.55)	3.35 (0.30)	−0.21
Caudate	4.11 (0.40)	3.83 (0.17)	0.74*
Putamen	4.00 (0.32)	3.83 (0.22)	0.56*
Pallidum	3.96 (0.36)	3.84 (0.21)	0.38
Thalamus	4.02 (0.34)	3.96 (0.24)	0.20

Table 2
Damping ratio, ξ, of cerebral lobes and subcortical gray matter structures in adolescents and adults, and Cohen's d effect size indicating the difference between populations. Values presented as population mean (standard deviation). Significant differences are marked with *.

Region	Adolescent ξ	Adult ξ	Cohen's d
Cerebrum	0.225 (0.021)	0.222 (0.018)	0.14
Cerebellum	0.286 (0.050)	0.260 (0.042)	0.56*
Frontal Lobe	0.216 (0.022)	0.235 (0.029)	−0.80*
Occipital Lobe	0.269 (0.061)	0.271 (0.039)	−0.03
Parietal Lobe	0.247 (0.034)	0.243 (0.040)	0.11
Temporal Lobe	0.237 (0.034)	0.220 (0.024)	0.61*
Deep GM/WM	0.218 (0.024)	0.208 (0.019)	0.47
Amygdala	0.228 (0.039)	0.215 (0.032)	0.19
Hippocampus	0.188 (0.032)	0.187 (0.030)	0.01
Caudate	0.205 (0.028)	0.221 (0.017)	−0.65*
Putamen	0.209 (0.020)	0.221 (0.010)	−0.63*
Pallidum	0.199 (0.017)	0.203 (0.018)	−0.25
Thalamus	0.192 (0.019)	0.187 (0.012)	0.22

(11.5%–31.3% percent stiffer). The caudate, putamen, pallidum, and thalamus did not differ from each other, but each were stiffer than structures of the medial temporal lobe, the hippocampus and amygdala.

3.2. Damping ratio

Fig. 3 presents ξ values for both cerebral lobes and subcortical gray matter structures in our adolescent population, which are also shown in Table 2. The cerebellum and occipital lobes had the highest ξ and were significantly different from all other reported structures ($p < 0.001$). The deep GM/WM, partially made up of the subcortical structures, had the lowest ξ (0.218). Of the individual subcortical structures, the hippocampus has the lowest ξ (0.188). Only the hippocampus, pallidum, and thalamus were significantly different than the cerebrum.

3.3. Comparison with the adult brain

Fig. 4 presents the comparison of adolescent and adult regional stiffness values. The cerebrum was found to have similar stiffness in adolescents and adults (3.13 v. 3.23 kPa; −3.1%), but the cerebellum, parietal, and temporal lobes were significantly different in adolescents and adults ($p < 0.01$). The temporal and parietal lobes were significantly less stiff in adolescents than adults (−4.8% and −9.0% softer, respectively), while the frontal lobe met only trend-level significance (2.97 v. 3.11 kPa; −4.5%). The occipital lobe was of comparable stiffness in adolescents and adults (2.80 v. 2.76 kPa). Interestingly, the deep GM/WM region was not significantly different, but the caudate (4.11 v. 3.83; 7.3%) and putamen (4.00 v. 3.83; 4.4%), which are located in the deep GM/WM, are significantly stiffer in adolescents. The hippocampus and amygdala were not significantly different between groups, but in both groups the hippocampus and amygdala were significantly less stiff than the other subcortical structures. Larger variability in measurements was seen in the adolescent group for all subcortical structures but variability was comparable among lobes.

Fig. 5 shows the damping ratio comparison of adolescents and adults for A) lobes and B) subcortical gray matter structures. The cerebrum ξ was similar for both adolescents and adults (0.225 v. 0.222; 1.4%). Similar regions showed significant difference between groups in μ: cerebellum and temporal lobe both had higher ξ in adolescents, while frontal lobe ξ was lower in adolescents (0.216 v. 0.235; −8.1%). The caudate and putamen were also significantly lower ξ in adolescents compared to adults (−7.2% and −5.4%, respectively).

4. Discussion

In this work, we present a detailed characterization of the viscoelastic mechanical properties (stiffness, μ, and damping ratio, ξ) of the healthy adolescent brain, as measured with MRE. In addition to measuring properties of the overall cerebrum and cerebellum, we determined the regional properties of cerebral lobes (frontal, occipital, parietal, and temporal) and subcortical gray matter structures (amygdala, hippocampus, caudate, putamen, pallidum, and thalamus). By comparing different regions within the adolescent brain, we found similar trends as reported for adults (Johnson et al., 2016; Murphy et al., 2013) and observed in the adult population considered in this work. The cerebellum was significantly softer than the cerebrum while the deep gray and white matter was significantly stiffer, and the cerebral

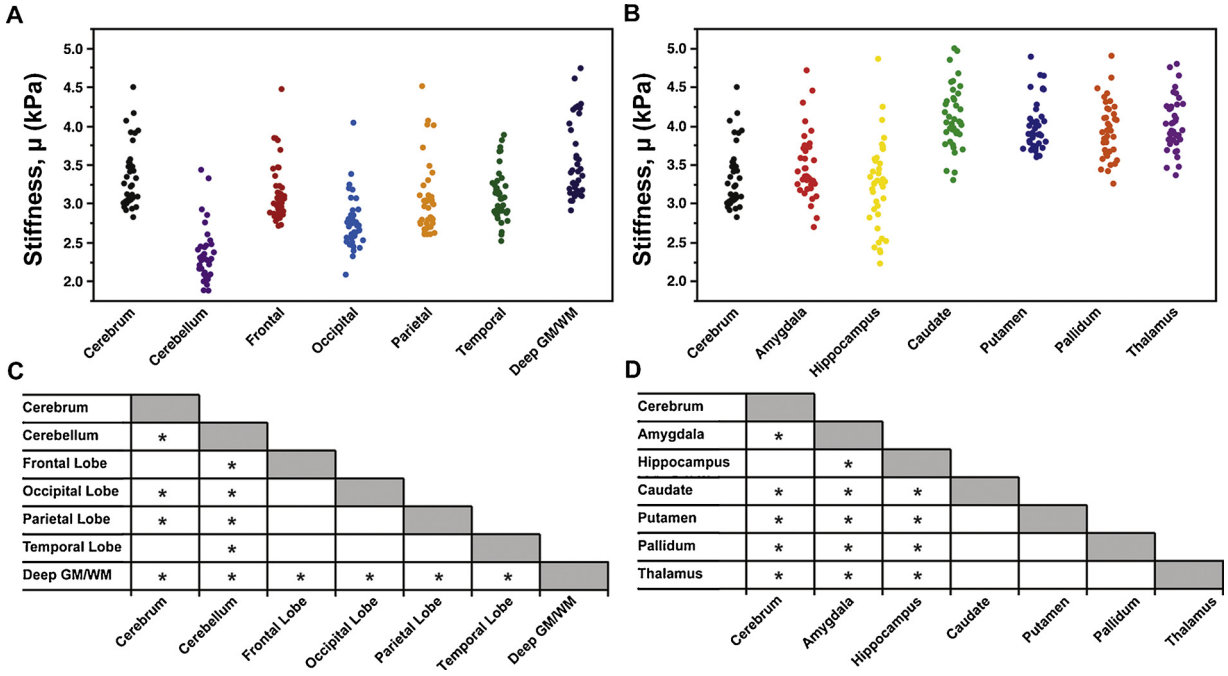

Fig. 2. Shear stiffness, μ, of (A) cerebral lobes and (B) subcortical gray matter structures of 40 adolescent brain MRE subjects, and charts indicating significant differences among pairs of structures. All measures are at 50 Hz.

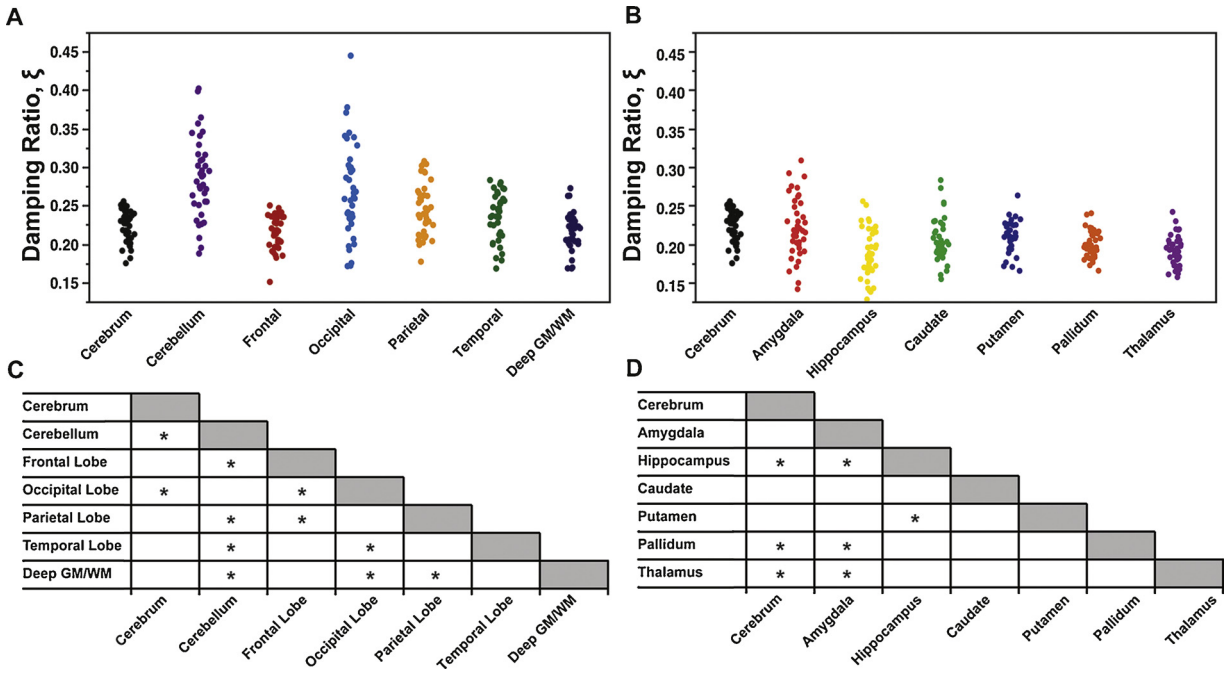

Fig. 3. Damping ratio, ξ, of (A) cerebral lobes and (B) subcortical gray matter structures of 40 adolescent brain MRE subjects, and charts indicating significant differences among pairs of structures. All measures are at 50 Hz.

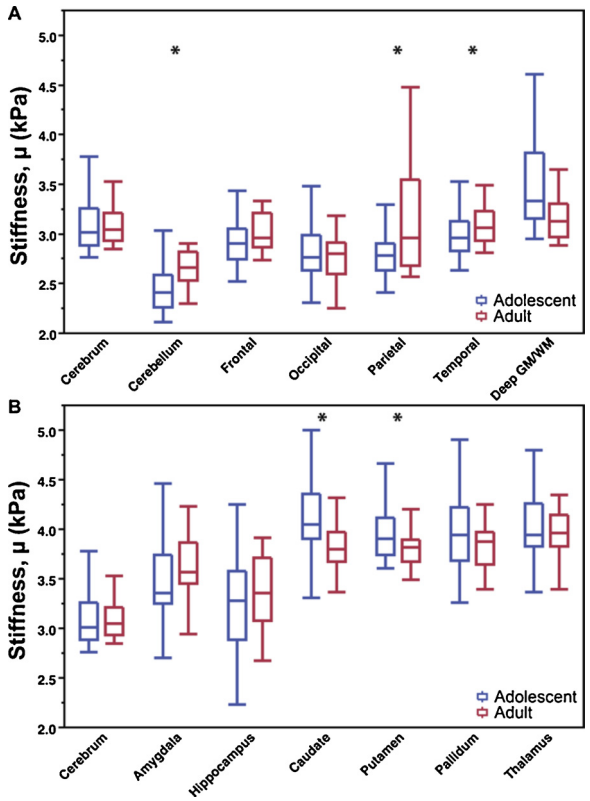

Fig. 4. Comparison of adolescent shear stiffness, μ, with adult shear stiffness in (A) cerebral lobe regions and (B) subcortical gray matter structures.

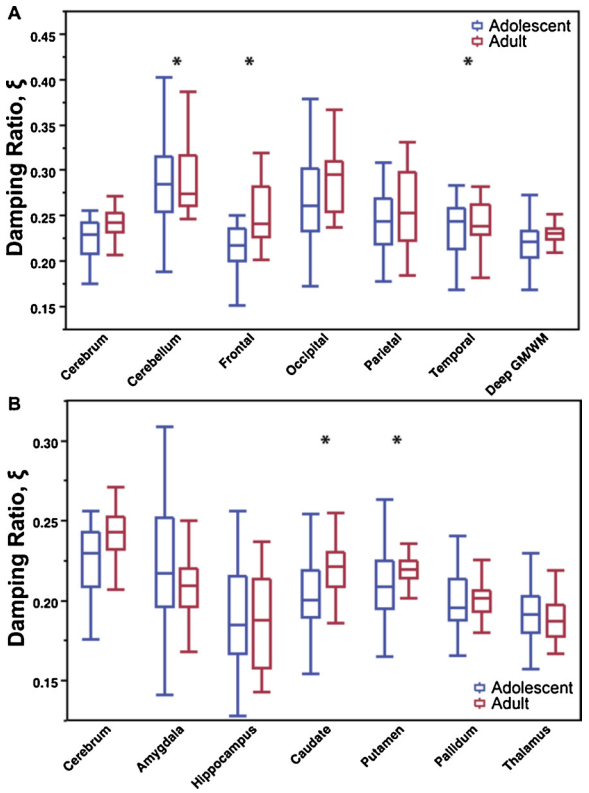

Fig. 5. Comparison of adolescent damping ratio, ξ, with adult damping ratio in (A) cerebral lobe regions and (B) subcortical gray matter structures.

lobes did not significantly differ from each other. Additionally, subcortical gray matter structures were generally stiffer than the cerebrum, while the amygdala and hippocampus of the medial temporal lobe exhibited separate patterns of stiffness and damping ratio study.

We also compared adolescent mechanical properties to those of the adult brain; data for which was collected as part of another study (Johnson et al., 2016) under identical protocol and reprocessed simultaneously with the adolescent data presented in this paper. Although we expect stiffness differences between adolescents and adults, we do not expect that the process of obtaining the MRE data will be affected by physiological size differences in adolescents. At the age of puberty, as analyzed in this paper, cranial volume and circumference

are nearly the same as in adults (Bartholomeusz et al., 2002), and we expect the wave propagation characteristics to be similar between population. Additionally, the calculation of viscoelastic properties through mechanical inversion is not influenced by the amplitude of shear waves as long as there is adequate strain and signal-to-noise ratio (McGarry et al., 2011), which we confirmed in our data. This allows us to directly compare mechanical properties of adolescent and adult brains through MRE.

Comparing adolescent brain stiffness to adult brain stiffness revealed several interesting trends. Despite no significant difference in overall cerebrum stiffness between adolescents and adults, the large cerebral lobe regions (temporal, parietal, and frontal) were generally softer relative to the overall cerebrum in adolescents. This suggests a potential gradient in stiffness from the periphery of the brain being softer and the interior stiffer in adolescents. This finding may be in part explained by the decrease in cortical gray matter volume and increase in white matter volume during this developmental period (Gogtay et al., 2004; Paus et al., 2001), with white matter being stiffer than gray and thus resulting in a stiffening of the lobe regions. When comparing the damping ratio of the same regions, we find that only the temporal (higher) and frontal (lower) significantly differ from the others. This may be related to differences in developmental trajectory between the regions, as white matter maturation and cortical thickness changes vary across lobes (Tamnes et al., 2010).

Of the subcortical gray matter regions, the caudate and putamen exhibited significantly greater stiffness in adolescents. The hippocampus and amygdala that comprise the medial temporal lobe, were seen in both groups to be significantly less stiff than the other subcortical structures but not significantly different between groups. Both the hippocampus and amygdala exhibit a protracted development period with regards to increasing structure volume relative to other subcortical regions (Goddings et al., 2014; Wierenga et al., 2014), which may be why these structures have different stiffness than the other regions (see Fig. 2) and do not exhibit the same relationships with the adult brain (see Fig. 4). However, this does not explain why the caudate and putamen are stiffer in adolescents than in adults if these regions are nearer to maturity, though these dynamics may be related to the complex structural reorganization in these regions occurring after they have reached peak volume (Goddings et al., 2014; Raznahan et al., 2014).

The damping ratio, ξ, is a unitless measure of relative viscoelastic behavior of tissue, though it is not commonly reported in the brain MRE literature. Tissue viscosity, in general, is expected to reflect geometrical or organizational aspects of brain tissue microstructure (Sack et al., 2013). In our adolescent population, we find that ξ of subcortical gray matter structures are, in general, similar to those in an adult population with two exceptions: caudate and putamen ξ are lower in adolescents, which again is likely indicative of different stages of development captured in this cross-sectional study. Despite damping ratio (or other viscosity measures) being less commonly reported in the brain MRE literature, it may be of particular interest in examining brain development as it relates to cognitive function, and our group has recently reported on the sensitivity of the damping ratio of the hippocampus to memory performance (Schwarb et al., 2017, 2016).

This study had several limitations. We only examined adolescents with a limited age range (12–14) that precluded analysis of how the mechanical properties of the brain develop from childhood to adolescence and into young adulthood. A more diverse age group, as well as longitudinal measurements in the same participants, is needed to gain a more complete understanding of mechanical structural changes throughout development. Such studies may also consider how MRE measures provide complementary information to other biophysical imaging parameters (*e.g.* from diffusion MRI). Additionally, we also used a 2.0 mm isotropic resolution for this study to reduce the scan time for the adolescent population. We have recently demonstrated that this resolution has minimal impact on average population values in subcortical gray matter structures (Johnson et al., 2016), though higher spatial resolution (*i.e.* 1.6 mm isotropic) improves sensitivity, and future studies examining structure-function relationships in the developing brain should consider using higher resolution.

5. Conclusion

This is the first report of the detailed mechanical properties of the human adolescent brain measured *in vivo* with MRE. By comparing regional values with adult brain values, we were able to observe differences in mechanical properties between the adolescent and adult brain. The results from this study provide baseline healthy adolescent data on regional brain stiffness which can eventually be used for examining the relationship between stiffness and various neurological conditions. MRE of the adolescent brain can be used to identify trends related to the development of brain structure and potentially provide insight into behavior and social development through sensitive structure-function relationships.

Conflict of interest

The authors report no conflicts of interest.

Acknowledgments

Support for this study was provided by NSF (SES-1459719), NIH/NIDA (R01-DA039923), the Delaware INBRE Program (NIH/NIGMS P20-GM103446), the Delaware CTR ACCEL Program (NIH/NIGMS U54-GM104941), NIH/NIBIB (R01-EB018230 and R01-EB001981), and NIH/NIMH (R01-MH062500).

Appendix A. Supplementary data

Supplementary material related to this article can be found, in the online version, at doi:https://doi.org/10.1016/j.dcn.2018.06.001.

References

Alonso-Ortiz, E., Levesque, I.R., Pike, G.B., 2015. MRI-based myelin water imaging: a technical review. Magn. Reson. Med. 73, 70–81. http://dx.doi.org/10.1002/mrm.25198.

Andersson, J.L.R., Smith, S.M., Jenkinson, M., 2008. FNIRT - FMRIB's non-linear image registration tool. In: Fourteenth Annu. Meet. Organ. Hum. Brain Mapping. Melbourne, Aust.

Arani, A., Murphy, M.C., Glaser, K.J., Manduca, A., Lake, D.S., Kruse, S.A., Jack, C.R., Ehman, R.L., Huston, J., 2015. Measuring the effects of aging and sex on regional brain stiffness with MR elastography in healthy older adults. Neuroimage 111, 59–64. http://dx.doi.org/10.1016/j.neuroimage.2015.02.016.

Bartholomeusz, H.H., Courchesne, E., Karns, C.M., 2002. Relationship between head circumference and brain volume in healthy normal toddlers, children, and adults. Neuropediatrics 33, 232–238.

Budday, S., Nay, R., de Rooij, R., Steinmann, P., Wyrobek, T., Ovaert, T.C., Kuhl, E., 2015. Mechanical properties of gray and white matter brain tissue by indentation. J. Mech. Behav. Biomed. Mater. 46, 318–330. http://dx.doi.org/10.1016/j.jmbbm.2015.02.024.

Freimann, F.B., Mueller, S., Streitberger, K.J., Guo, J., Rot, S., Ghori, A., Vajkoczy, P., Reiter, R., Sack, I., Braun, J., 2013. MR elastography in a murine stroke model reveals correlation of macroscopic viscoelastic properties of the brain with neuronal density. NMR Biomed. 26, 1534–1539. http://dx.doi.org/10.1002/nbm.2987.

Goddings, A.L., Mills, K.L., Clasen, L.S., Giedd, J.N., Viner, R.M., Blakemore, S.J., 2014. The influence of puberty on subcortical brain development. Neuroimage 88, 242–251. http://dx.doi.org/10.1016/j.neuroimage.2013.09.073.

Gogtay, N., Giedd, J.N., Lusk, L., Hayashi, K.M., Greenstein, D., Vaituzis, aC., Nugent, T.F., Herman, D.H., Clasen, L.S., Toga, A.W., Rapoport, J.L., Thompson, P.M., 2004. Dynamic mapping of human cortical development during childhood through early adulthood. Proc. Natl. Acad. Sci. U. S. A. 101, 8174–8179. http://dx.doi.org/10.1073/pnas.0402680101.

Hain, E.G., Klein, C., Munder, T., Braun, J., Riek, K., Mueller, S., Sack, I., Steiner, B., 2016. Dopaminergic neurodegeneration in the mouse is associated with decrease of viscoelasticity of substantia nigra tissue. PLoS One 11, e0161179. http://dx.doi.org/10.1371/journal.pone.0161179.

Hiscox, L.V., Johnson, C.L., Barnhill, E., McGarry, M.D.J., Huston, J., van Beek, E.J.R., Starr, J.M., Roberts, N., 2016. Magnetic resonance elastography (MRE) of the human brain: technique, findings and clinical applications. Phys. Med. Biol. 61, R401–R437.

http://dx.doi.org/10.1088/0031-9155/61/24/R401.
Hiscox, L.V., Johnson, C.L., McGarry, M.D.J., Perrins, M., Littlejohn, A., van Beek, E.J.R., Roberts, N., Starr, J.M., 2018. High-resolution magnetic resonance elastography reveals differences in subcortical gray matter viscoelasticity between young and healthy older adults. Neurobiol. Aging 65, 158–167. http://dx.doi.org/10.1016/j.neurobiolaging.2018.01.010.
Jenkinson, M., Bannister, P., Brady, M., Smith, S., 2002. Improved optimization for the robust and accurate linear registration and motion correction of brain images. Neuroimage 17, 825–841. http://dx.doi.org/10.1016/S1053-8119(02)91132-8.
Jenkinson, M., Beckmann, C.F., Behrens, T.E.J., Woolrich, M.W., Smith, S.M., 2012. FSL Neuroimage 62, 782–790. http://dx.doi.org/10.1016/j.neuroimage.2011.09.015.
Johnson, C.L., Telzer, E.H., 2017. Magnetic resonance elastography for examining developmental changes in the mechanical properties of the brain. Dev. Cogn. Neurosci. http://dx.doi.org/10.1016/j.dcn.2017.08.010. in press.
Johnson, C.L., Holtrop, J.L., McGarry, M.D.J., Weaver, J.B., Paulsen, K.D., Georgiadis, J.G., Sutton, B.P., 2014. 3D multislab, multishot acquisition for fast, whole-brain MR elastography with high signal-to-noise efficiency. Magn. Reson. Med. 71, 477–485. http://dx.doi.org/10.1002/mrm.25065.
Johnson, C.L., Schwarb, H., D.J. McGarry, M., Anderson, A.T., Huesmann, G.R., Sutton, B.P., Cohen, N.J., 2016. Viscoelasticity of subcortical gray matter structures. Hum. Brain Mapp. 37, 4221–4233. http://dx.doi.org/10.1002/hbm.23314.
Johnson, C.L., Schwarb, H., Horecka, K.M., McGarry, M.D.J., Hillman, C.H., Kramer, A.F., Cohen, N.J., Barbey, A.K., 2018. Double dissociation of structure-function relationships in memory and fluid intelligence observed with magnetic resonance elastography. Neuroimage 171, 99–106. http://dx.doi.org/10.1016/j.neuroimage.2018.01.007.
Klein, C., Hain, E.G., Braun, J., Riek, K., Mueller, S., Steiner, B., Sack, I., 2014. Enhanced adult neurogenesis increases brain stiffness: in vivo magnetic resonance elastography in a mouse model of dopamine depletion. PLoS One 9, e92582. http://dx.doi.org/10.1371/journal.pone.0092582.
Lebel, C., Treit, S., Beaulieu, C., 2017. A review of diffusion MRI of typical white matter development from early childhood to young adulthood. NMR Biomed. http://dx.doi.org/10.1002/nbm.3778. in press.
Lenroot, R.K., Giedd, J.N., 2006. Brain development in children and adolescents: insights from anatomical magnetic resonance imaging. Neurosci. Biobehav. Rev. 30, 718–729. http://dx.doi.org/10.1016/j.neubiorev.2006.06.001.
Maldjian, J.A., Laurienti, P.J., Kraft, R.A., Burdette, J.H., 2003. An automated method for neuroanatomic and cytoarchitectonic atlas-based interrogation of fMRI data sets. Neuroimage 19, 1233–1239. http://dx.doi.org/10.1016/S1053-8119(03)00169-1.
Manduca, A., Oliphant, T.E., Dresner, M.A., Mahowald, J.L., Kruse, S.A., Amromin, E., Felmlee, J.P., Greenleaf, J.F., Ehman, R.L., 2001. Magnetic resonance elastography: non-invasive mapping of tissue elasticity. Med. Image Anal. 5, 237–254.
Mariappan, Y.K., Glaser, K.J., Richard, L., Ehman, 2010. Magnetic resonance elastography: a review. Clin. Anat. 23, 497–511. http://dx.doi.org/10.1002/ca.21006.MAGNETIC.
McGarry, M.D.J., Van Houten, E.E.W., 2008. Use of a Rayleigh damping model in elastography. Med. Biol. Eng. Comput. 46, 759–766. http://dx.doi.org/10.1007/s11517-008-0356-5.
McGarry, M.D.J., Van Houten, E.E.W., Perrîez, P.R., Pattison, A.J., Weaver, J.B., Paulsen, K.D., 2011. An octahedral shear strain-based measure of SNR for 3D MR elastography. Phys. Med. Biol. 56, N153–N164. http://dx.doi.org/10.1088/0031-9155/56/13/N02.
McGarry, M.D.J., Van Houten, E.E.W., Johnson, C.L., Georgiadis, J.G., Sutton, B.P., Weaver, J.B., Paulsen, K.D., 2012. Multiresolution MR elastography using nonlinear inversion. Med. Phys. 39, 6388–6396. http://dx.doi.org/10.1118/1.4754649.
McGarry, M., Johnson, C.L., Sutton, B.P., Van Houten, E.E., Georgiadis, J.G., Weaver, J.B., Paulsen, K.D., 2013. Including spatial information in nonlinear inversion MR elastography using soft prior regularization. IEEE Trans. Med. Imaging 32, 1901–1909. http://dx.doi.org/10.1109/TMI.2013.2268978.
Murphy, M.C., Huston, J., Jack, C.R., Glaser, K.J., Senjem, M.L., Chen, J., Manduca, A., Felmlee, J.P., Ehman, R.L., 2013. Measuring the characteristic topography of brain stiffness with magnetic resonance elastography. PLoS One 8, e81668. http://dx.doi.org/10.1371/journal.pone.0081668.
Murphy, M.C., Jones, D.T., Jack, C.R., Glaser, K.J., Senjem, M.L., Manduca, A., Felmlee, J.P., Carter, R.E., Ehman, R.L., Huston, J., 2016. Regional brain stiffness changes across the Alzheimer's disease spectrum. NeuroImage Clin. 10, 283–290. http://dx.doi.org/10.1016/j.nicl.2015.12.007.
Muthupillai, R., Lomas, D.J., Rossman, P.J., Greenleaf, J.F., Manduca, A., Ehman, R.L., 1995. Magnetic resonance elastography by direct visualization of propagating acoustic strain waves. Science 269, 1854–1857.
Patenaude, B., Smith, S.M., Kennedy, D.N., Jenkinson, M., 2011. A Bayesian model of shape and appearance for subcortical brain segmentation. Neuroimage 56, 907–922. http://dx.doi.org/10.1016/j.neuroimage.2011.02.046.
Paus, T., Collins, D.L., Evans, A.C., Leonard, G., Pike, B., Zijdenbos, A., 2001. Maturation of white matter in the human brain: a review of magnetic resonance studies. Brain Res. Bull. 54, 255–266. http://dx.doi.org/10.1016/S0361-9230(00)00434-2.
Raznahan, A., Shaw, P.W., Lerch, J.P., Clasen, L.S., Greenstein, D., Berman, R., Pipitone, J., Chakravarty, M.M., Giedd, J.N., 2014. Longitudinal four-dimensional mapping of subcortical anatomy in human development. Proc. Natl. Acad. Sci. U. S. A. 111, 1592–1597. http://dx.doi.org/10.1073/pnas.1316911111.
Romano, A.J., Scheel, M., Hirsch, S., Braun, J., Sack, I., 2012. In vivo waveguide elastography of white matter tracts in the human brain. Magn. Reson. Med. 68, 1410–1422. http://dx.doi.org/10.1002/mrm.24141.
Sack, I., Streitberger, K.J., Krefting, D., Paul, F., Braun, J., 2011. The influence of physiological aging and atrophy on brain viscoelastic properties in humans. PLoS One 6, e23451. http://dx.doi.org/10.1371/journal.pone.0023451.
Sack, I., Jöhrens, K., Würfel, J., Braun, J., 2013. Structure-sensitive elastography: on the viscoelastic powerlaw behavior of in vivo human tissue in health and disease. Soft Matter 9, 5672–5680. http://dx.doi.org/10.1039/c3sm50552a.
Schregel, K., Wuerfel, E., Garteiser, P., Gemeinhardt, I., Prozorovski, T., Aktas, O., Merz, H., Petersen, D., Wuerfel, J., Sinkus, R., 2012. Demyelination reduces brain parenchymal stiffness quantified in vivo by magnetic resonance elastography. Proc. Natl. Acad. Sci. U. S. A. 109, 6650–6655. http://dx.doi.org/10.1073/pnas.1200151109.
Schwarb, H., Johnson, C.L., McGarry, M.D.J., Cohen, N.J., 2016. Medial temporal lobe viscoelasticity and relational memory performance. Neuroimage 132, 534–541. http://dx.doi.org/10.1016/j.neuroimage.2016.02.059.
Schwarb, H., Johnson, C.L., Daugherty, A.M., Hillman, C.H., Kramer, A.F., Cohen, N.J., Barbey, A.K., 2017. Aerobic fitness, hippocampal viscoelasticity, and relational memory performance. Neuroimage 153, 179–188. http://dx.doi.org/10.1016/j.neuroimage.2017.03.061.
Shreiber, D.I., Hao, H., Elias, R.A., 2009. Probing the influence of myelin and glia on the tensile properties of the spinal cord. Biomech. Model. Mechanobiol. 8, 311–321. http://dx.doi.org/10.1007/s10237-008-0137-y.
Streitberger, K.J., Sack, I., Krefting, D., Pfüller, C., Braun, J., Paul, F., Wuerfel, J., 2012. Brain viscoelasticity alteration in chronic-progressive multiple sclerosis. PLoS One 7, e29888. http://dx.doi.org/10.1371/journal.pone.0029888.
Tamnes, C.K., Østby, Y., Fjell, A.M., Westlye, L.T., Due-Tønnessen, P., Walhovd, K.B., 2010. Brain maturation in adolescence and young adulthood: regional age-related changes in cortical thickness and white matter volume and microstructure. Cereb. Cortex 20, 534–548. http://dx.doi.org/10.1093/cercor/bhp118.
Toga, A.W., Thompson, P.M., Sowell, E.R., 2006. Mapping brain maturation. Trends Neurosci. 29, 148–159. http://dx.doi.org/10.1016/j.tins.2006.01.007.
Van Houten, E.E.W., Miga, M.I., Weaver, J.B., Kennedy, F.E., Paulsen, K.D., 2001. Three-dimensional subzoned-based reconstruction algorithm for MR elastography. Magn. Reson. Med. 45, 827–837. http://dx.doi.org/10.1002/mrm.1111.
Wang, Y., 2012. Imaging of myelination. J. Med. Chem. 55, 94–105. http://dx.doi.org/10.1021/jm201010e.Myelin.
Weickenmeier, J., de Rooij, R., Budday, S., Ovaert, T.C., Kuhl, E., 2017. The mechanical importance of myelination in the central nervous system. J. Mech. Behav. Biomed. Mater. 76, 119–124. http://dx.doi.org/10.1016/j.jmbbm.2017.04.017.
West, K.L., Kelm, N.D., Carson, R.P., Gochberg, D.F., Ess, K.C., Does, M.D., 2016. Myelin volume fraction imaging with MRI. Neuroimage. http://dx.doi.org/10.1016/j.neuroimage.2016.12.067. in press.
Wierenga, L., Langen, M., Ambrosino, S., van Dijk, S., Oranje, B., Durston, S., 2014. Typical development of basal ganglia, hippocampus, amygdala and cerebellum from age 7 to 24. Neuroimage 96, 67–72. http://dx.doi.org/10.1016/j.neuroimage.2014.03.072.
Wuerfel, J., Paul, F., Beierbach, B., Hamhaber, U., Klatt, D., Papazoglou, S., Zipp, F., Martus, P., Braun, J., Sack, I., 2010. MR-elastography reveals degradation of tissue integrity in multiple sclerosis. Neuroimage 49, 2520–2525. http://dx.doi.org/10.1016/j.neuroimage.2009.06.018.
Zhang, Y., Brady, M., Smith, S., 2001. Segmentation of brain MR images through a hidden Markov random field model and the expectation-maximization algorithm. IEEE Trans. Med. Imaging 20, 45–57. http://dx.doi.org/10.1109/42.906424.
Zhang, J., Green, M.A., Sinkus, R., Bilston, L.E., 2011. Viscoelastic properties of human cerebellum using magnetic resonance elastography. J. Biomech. 44, 1909–1913. http://dx.doi.org/10.1016/j.jbiomech.2011.04.034.